THE USE OF HYPERSPECTRAL REMOTE SENSING DATA FOR THE ASSESSMENT OF CHEMICAL PROPERTIES OF DRYLAND SOILS IN SE-SPAIN

Thomas Jarmer[1], Joachim Hill[2] and Sebastian Mader[3]

1. Freie Universität Berlin; Remote Sensing and Geoinformatics, Institute for Geographical Sciences D-12249 Berlin, Germany; jarmer@geog.fu-berlin.de
2. Remote Sensing Department, University of Trier, D-54286 Trier, Germany, hillj@uni-trier.de
3. Remote Sensing Department, University of Trier, D-54286 Trier, Germany, mader@uni-trier.de

ABSTRACT

Soil samples were collected in the catchment of the upper Rio Guadalentin basin in SE Spain (Prov. Murcia). Additional to soil chemical laboratory analysis the spectral reflectance of the soil samples was measured in the range of 0.35 and 2.5 µm. These reflectance measurements were convex-hull-normalised to derive individual absorption features. The continuous spectra were used to calculate colour parameters according to the Commission Internationale de l´Eclairage (CIE) colour scheme. Accordingly, a method for spectral detection of pedo-chemical properties in the investigated soil was developed based on statistical analysis which allows the prediction of the chemical concentrations in soils. Organic carbon contents were estimated from reflectance measurements based on C.I.E. colour coordinates with high accuracy ($r^2_{cv} > 0.79$). Inorganic carbon was predicted from laboratory reflectance measurements with an accuracy of $r^2_{cv} > 0.71$ considering the normalized absorption area of the carbonate absorption feature at 2.33 µm and the C.I.E. chromaticity value x and y. The transfer of the derived regression models to HyMap data allowed for the spatial prediction of organic and inorganic carbon contents in the Rio Guadalentin basin. Concentrations obtained are in accordance with the concentration range of the chemical analysis. The predicted chemical soil concentrations reflect the physio-geographic conditions of the investigated area.

INTRODUCTION

Three decades after the first United Nations Conference on Desertification 1977 in Nairobi reduction of soil and water resources and associated land degradation processes world-wide are considered as one of the most important environmental problems. It is agreed that land degradation processes are climate sensitive and related to physio-geographical and anthropogenic conditions (i). Regarding the fact that the pressure on arid and semi-arid areas resulting from climatic variability, climate change, demands of increasing stocking rates and population development was probably never as high as nowadays (ii), arid and semi-arid environments are often considered as risk areas in the context of global climate change and desertification dynamics.

Soils as a substantial part of terrestrial ecosystems are extremely important, since soils are. Soil chemical and physical properties are basic indicators for soil productivity which is strongly related to agricultural production. In semi-arid and arid environments the inorganic carbon content in soils developed on carbonatic bedrock material is a major soil development indicator. High inorganic carbon concentrations point to weakly developed or degraded soils while low contents often indicate more developed soils. Organic carbon is a second reliable indicator related to soil quality and depending on water availability. In drylands water is the limiting factor for vegetation growth and influences organic matter production. Increasing soil organic carbon concentrations improve soil conditions because of better aggregation, higher infiltration rates and water retention which are conductive to their resistance to erosion.

Since the spatial detection of organic and inorganic carbon is of great importance in the context of land degradation monitoring and sub-recent morphodynamics, it is necessary to develop a remote sensing based approach for spectral determination of soil organic and inorganic carbon concentrations. Consequently, it is the major objective of this study to investigate the potential of hyperspectral imagery for this purpose and to develop an approach for the spatial assessment of these important pedo-chemical parameters.

STUDY SITE

The study site is located in the upper watershed of the Rio Guadalentin in SE-Spain (Prov. Murcia) and belongs to the Cordillera Betica (Figure 1). The lithology is dominated by limestone and marls.

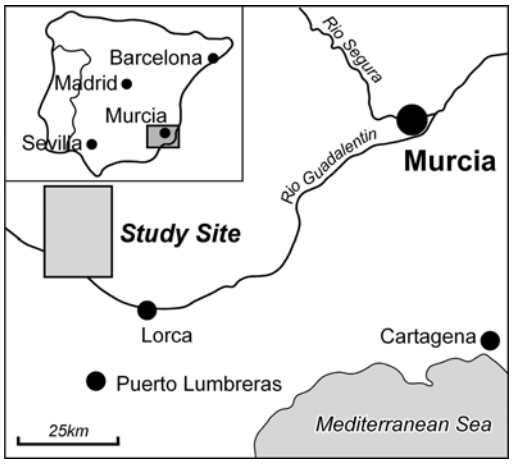

Figure 1: Location of the study site

Southeast Spain is one of the driest areas of the Mediterranean Basin. Mean annual rainfall amount in the lowlands of the Guadalentin basin is around 300mm while in the surrounding mountain ranges annual rainfall amounts can exceed 1000mm (iii). The actual study site is characterised by an average precipitation amount of approx. 180mm due to the lee location south of the Sierra Gigante. Following the FAO classification scheme, soils are mainly Lithosols and Calcaric Regosols. Since soil development according to the prevailing semi-arid climatic conditions is low, variations in soil colour and soil structure are limited and mostly related to characteristics of bedrock material. Dryland farming of several crop types dominates the valleys. The hills and areas which are not under agricultural use are mostly covered by *Stipa tenacissima* and *Rosmarinus officinalis*. Besides, mainly at higher altitudes, pines (*Pinus halepensis*) occur.

METHODS

Field sampling and chemical analysis

To establish a relationship between soil reflectance properties and soil organic and inorganic carbon content based on statistical methods, a number of soil samples were collected along several transects in the field. In order to assess the spatial variability of the soil properties induced by local relief, the sampling transects were positioned along directions for which local physiogeographic gradients (e.g. differences in surface flow) could be assumed. North- as well as South-facing ridges and valley bottoms were crossed by the five different topographical transects illustrated in Figure 2.

For each position (n = 77), an integrative sample was taken from the upper 2 cm of the soil profile representing an area of about 1 m². The soil samples were air-dried in the laboratory, gently crushed in order to pass a 2 mm-sieve and carefully homogenized. The total amounts of soil organic carbon and soil inorganic carbon were measured with a Leco-RC 412 analyser.

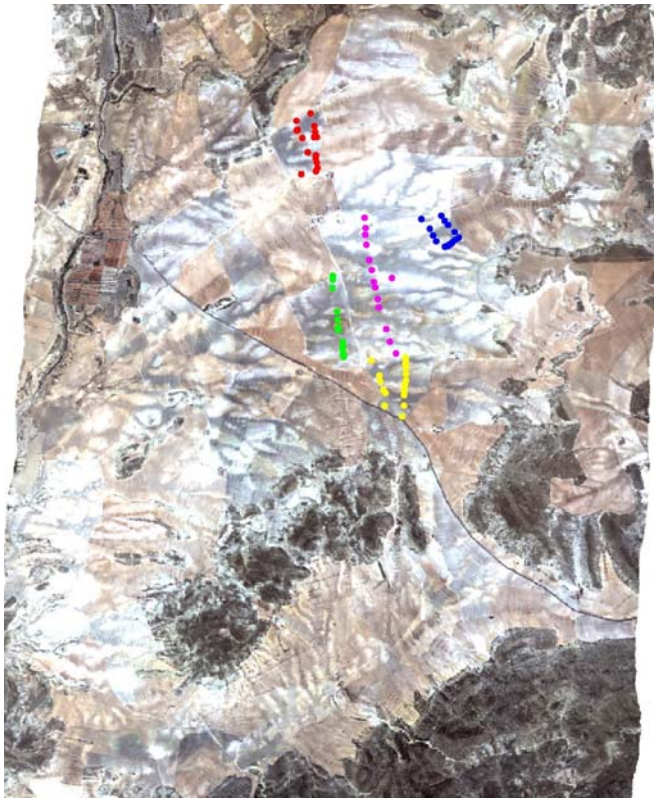

Figure 2: The location of the five different sampling transects relative to the HyMap data. Each transect is shown in a different colour.

Reflectance measurements

The bi-directional reflectance measurements of the soil samples were acquired in the laboratory with an ASD FieldSpec-II spectroradiometer (Analytical Spectral Devices). Spectral readings were taken at 1 nm steps between 350 nm and 2500 nm using a reflectance standard of known reflectivity (Spectralon©). A 1000 W quartz-halogen lamp set at a distance of approximately 30 cm was used for illumination. The illumination zenith angle was adjusted to 30 degrees. The optical head of the spectroradiometer was mounted on a tripod in nadir position at a distance of 10 cm to the sample.

Absolute bi-directional reflectance spectra were obtained by multiplying the raw reflectance spectra by the certified reflectivity of the Spectralon panel. No data pre-processing was applied; however, only the spectral range from 0.4 to 2.4 µm was used for further study to exclude the noisy parts of the spectra.

Organic carbon and inorganic carbon in soils have a strong influence on the soil reflectance in the visible domain (e.g. iv). In general, with increasing organic matter content soil reflectance decreases in the wavelength range 0.4 – 2.5 µm (v). An increase of reflectance with rising contents of inorganic carbon often is observed. Therefore, it was decided to include colour information in the spectral analysis. For the calculation of colour parameters, the reflectance measurements were converted to trichromatic specifications, and then expressed in terms of the „Commission Internationale de ´Eclairage [C.I.E.]“ colour notation (Y, x, y) of 1931. In this colour system the colour intensity is characterised by the tristimulus value “Y” (luminance), which represents the brightness of colour while “x” and “y” are the chromaticity coordinates (vi, vii). The C.I.E. colour coordinates were already found to contain substantial information for spectroradiometric detection of organic and inorganic carbon (viii, ix).

Furthermore, carbonates are known to show a diagnostic vibrational absorption band in the Near Infrared at 2.30 - 2.35 µm (x, xi). Hence, individual spectral features (maximum absorption depth,

absorption width and area integrals) for this absorption band were derived from the measured reflectance spectra using the continuum removal approach.

The C.I.E. colour coordinates and the derived absorption features were used to build multivariate linear regression models for the prediction of the above mentioned soil chemical properties from spectral reflectance. The performance of several models based on different linear combinations of the derived spectral features was first tested by cross validating the results. For each of the two soil properties to be estimated, one regression model was finally accepted and cross-validated according to the leave-one-out method. The coefficient of determination (r^2) and the root mean squared error (RMSE) were calculated to assess the prediction accuracy. Additionally, the relative root mean square error (rRMSE) was determined which is defined as the quotient of the RMSE and the mean of all samples. To assure the adequacy of the implemented regression model a t-test was applied to see whether the mean of the residuals was zero. Normal distribution of the residuals was verified by a Kolmogorov-Smirnov-test and auto-correlation of model residuals was ruled out by a Durbin-Watson-test. Subsequently, the final regression models were up-scaled to the hyperspectral image data of the HyMap sensor acquired for the test site.

Pre-processing of HyMap data

The geometric rectification of two HyMap images acquired for the test site on 29th June 2000 was accomplished using the parametric geocoding approach implemented by the PARGE software package (xii). The software uses navigation data collected during the flight to reconstruct the geometric properties of the acquired images. The navigational parameters collected during scene acquisition and used by the PARGE application were the aircraft's position, roll and pitch angles, as well as its heading and altitude above ground. One set of parameters was recorded for every image line scanned. The dynamics of both the collection of image and navigation data in combination with the uncertainties in the synchronization of both processes may cause inaccuracies in the rectified images. In the PARGE geocoding process, the navigation data are iteratively adjusted for these inaccuracies by using a set of ground control points. The software also uses a digital elevation model of the imaged area to account for terrain induced image distortions. To geocode the two images used in this work a total of 47 ground control points was collected by GPS measurements in the field. After geocoding, the images were resampled to a pixel size of 6 m, which is the approximate ground instantaneous field of view at nadir according to the aircrafts mean altitude above ground when acquiring the images. The positional accuracy of the individual pixel centres in the resulting products was estimated to be within about 7m in easting and northing for both images. The estimates are based on the residual errors after geocoding, as there was no additional set of ground control points available to independently validate the results.

After the geocoding of the individual HyMap scenes, the resulting images have been merged to produce one single image of larger coverage for further analysis. In the PARGE application, the coordinate system of the geocoded image product is determined by the properties of the digital elevation model used in the geocoding process. Since the subset of the elevation model was chosen large enough to cover both scenes and the same subset was used to geocode both images, the scenes could be merged by a simple masking operation without further resampling. The one of the two overlapping scenes acquired first showed a slightly better radiometric quality and was chosen as the base image. Merging the two scenes was accomplished by simply filling the raster of the first geocoded image with the grey values from the second image not overlapping with the first one.

Radiance calibration and atmospheric correction of the HyMap data acquired in the Guadalentin site was performed with the AtCPro radiative transfer code (xiii, xiv). The approach is based on the formulation of radiative transfer by Tanré et al. (xv); it provides corrections for atmospheric absorption, scattering and pixel adjacency effects, where diffusion and absorption processes are assumed to be independent and multiple scattering is accounted for according to Sobolev's approximate solution (xvi). Atmospheric extinction processes in the reflective optical domain are treated as a function of sensor and terrain altitude, and the absorbing gases (H_2O, O_3, CO_2, O_2, CH_4) are represented according to MODTRAN (xvii) gaseous transmittance data. The code allows

both, simulating atmospheric conditions and removing atmospheric distortions from radiance-calibrated remote sensing imagery. HyMap data have first been re-calibrated in flight by applying AtCPro in the forward mode for simulating the spectral at-sensor radiance for seven reflectance spectra from homogeneous reference surfaces in the field. Since no atmospheric measurements were taken during image acquisition, aerosol parameters and water vapour concentration had to be determined through an iterative approach with regard to the available ground reflectance data; finally, aerosol scattering was parameterised equivalent to a horizontal visibility of appr. 50 km, water vapour was estimated from the HyMap imagery itself according to an approach described in Hill & Mader (xviii). Using these estimated in-flight gain and offset coefficients the atmospheric correction produced high-quality reflectance spectra which permit a detailed analysis of the HyMap imagery.

Spectral unmixing analysis (e.g. (xix, xx) was used to determine fractions of vegetation, crop residuals and soil. Based on these results a soil mask was generated by determination of a threshold value to include only bare soil in the further analysis.

RESULTS AND DISCUSSION

Soil development is limited in the study area due to the relatively small average rainfall amount. The resulting shallow soils are strongly influenced by the characteristics of the bedrock material. Consequently, high concentrations of inorganic carbon were determined by chemical analysis ranging from less than 7.5 percent to more ten percent in the maximum. Furthermore, the semi-arid climatic conditions restrict vegetation growth and the production of organic matter. Hence, the soil samples are characterised by relatively low organic carbon concentrations which are below 0.7 percent at the average. Descriptive statistics of the investigated soil samples are summarized in Table 1.

Table 1: Descriptive statistics of organic carbon content of the soil samples for the study sites

	n	Min	Max	Mean	S.D.
C_{org} [%]	61	0.24	1.13	0.67	0.25
C_{inorg} [%]	77	7.43	10.24	9.11	0.70

For both, organic (C_{org}) and inorganic (C_{inorg}) carbon a statistically significant multivariate prediction model could be established from the laboratory reflectance measurements by using different combinations of the features derived from the measured spectra. In case of organic carbon the samples from one transect were excluded from further analysis.

For organic carbon, the following significant relationship was found:

$$C_{org} = 13.493-31.706*y-0.034*Y,$$

where C_{org} is given in percent, *y* is the CIE "y" chromaticity coordinate and *Y* represents the CIE luminance (brightness). This regression model explained cross-validated about 80 percent of the variance of soil organic carbon ($r^2_{cv} = 0.794$; $RMSE_{cv} = 0.110$).

The final model for prediction inorganic carbon from absorption parameters and C.I.E. colour coordinates results in a r_{cv}^2 of 0.715:

$$C_{inorg} = 43.12+44.535*x-142.246*y+0.480*a,$$

where C_{inorg} is given in percent, *x* is the CIE "x" chromaticity coordinate, *y* is the CIE "y" chromaticity coordinate, and *a* represents the total area of the diagnostic carbonate absorption feature centred at 2330 nm. This model performs well which is also indicated by a relatively low cross-validated root mean squared error of 0.609 and a low $rRMSE_{cv}$ of 0.067.

Figure 3 shows the cross validation results for the individual prediction models using the leave-one-out (jack-knifing) method. The linear regressions between the measured and modelled data for both soil variables show only a small offset and a gradient of almost unity. This near 1:1-relationship is an indication of the good performance of both models.

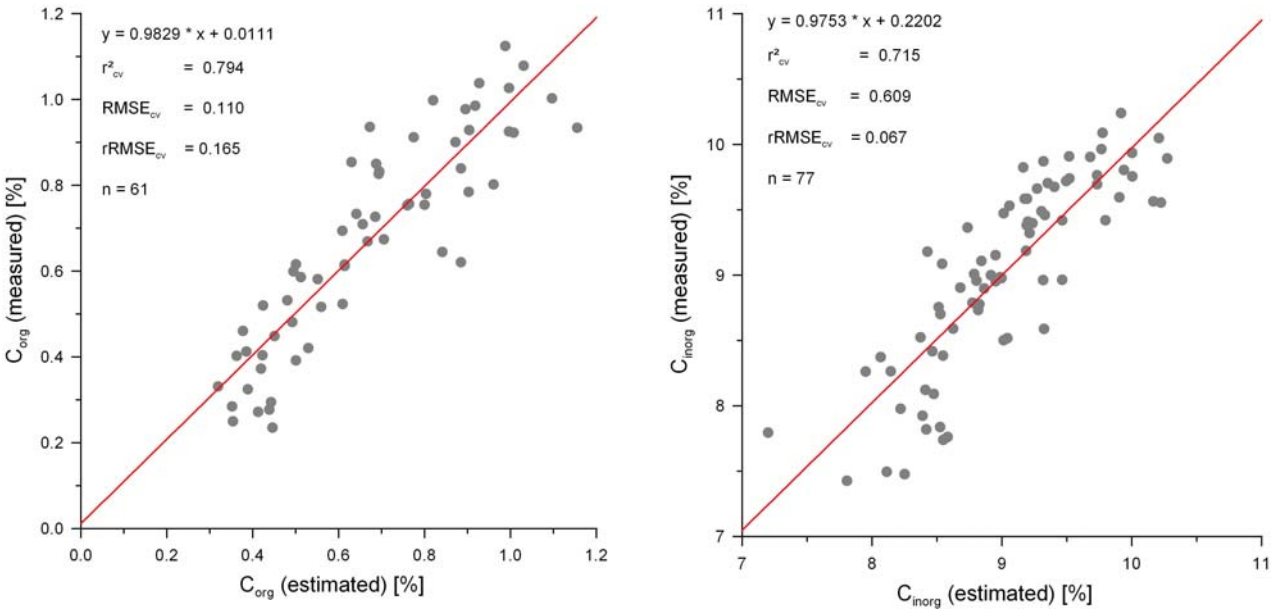

Figure 3: The results obtained by cross validating the individual prediction models for organic (left side) and inorganic (right side) carbon. The red line indicates the linear regression between the measured and modelled data for each variable.

For the spatially distributed prediction of soil organic and inorganic carbon contents, the spectral features used as parameters in the two prediction equations were computed from the spectral pixel vectors of the Guadalentin HyMap image. Thus, the organic and inorganic carbon content could be estimated for each pixel in the HyMap dataset by application of the respective prediction equation. The predicted percentages of organic and inorganic carbon for a subset of the HyMap image are shown in Figure 4.

Generally, the highest percentages of organic carbon in the imaged area are found in sinks and at valley bottoms, whereas low organic carbon contents occur on the ridges. In opposition to organic carbon, inorganic carbon contents are high in the vicinity of ridges and relatively low in sinks and at the bottom of valleys. Higher organic carbon concentrations at valley bottoms and in sinks are due to more favourable water supply in comparison to the ridges. Subsequently, conditions are more suitable for vegetation growth and organic material supply at the valley bottoms. On the same time the removal of carbonate is mainly influenced by the available amount of water which is indicated by lower inorganic carbon concentrations in these areas. At the ridges, less favourable water conditions limit soil development. Field survey indicated substantial surface flow at high intensity rainfall events. As a consequence less developed or degraded soils are more influenced by underlying bedrock material and hence, these areas are characterised by higher concentrations of inorganic carbon.

The value ranges obtained from the image data agree well with those of the laboratory samples, which are 0.24-1.13 percent for organic carbon and 7.43-10.24 percent for inorganic carbon (compare Figure 4; see also Table 1). To assess the accuracy of the spatially distributed estimates, the organic and inorganic carbon values obtained from the image data were validated with reference to the soil samples taken in the field. To compensate for up-scaling effects like uncertainties in sample location with respect to the image data, a 3x3 window of pixels centred on the coordinates of each field sample location was considered in the validation process. The validation was performed using the estimated pixel value within a window that best matched the

laboratory measurement of the corresponding sample collected in the field. The results of the validation step are illustrated in figure 5. For both variables, offset and gradient of the regression between the modelled and measured data are slightly higher compared to the validation results for the laboratory reflectance measurements, but still close to a linear 1:1-relationship. However, it has to be considered that this validation approach tends to overestimate the model fit.

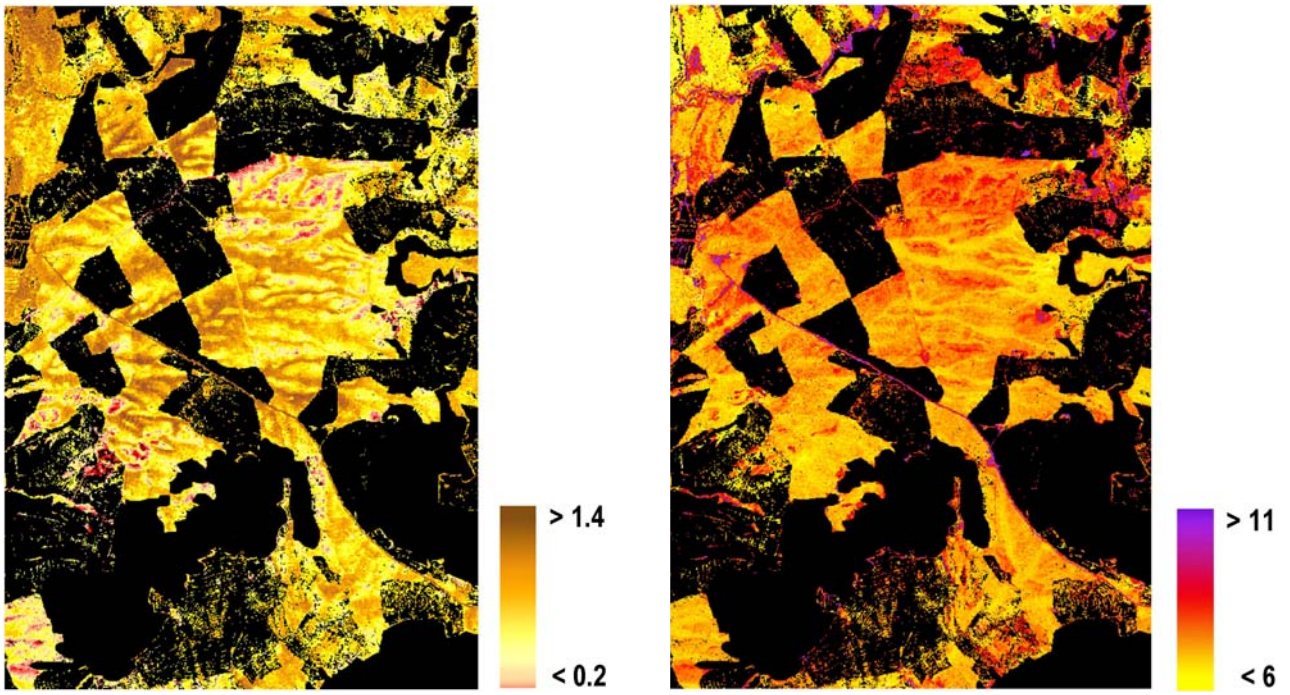

Figure 4: Predicted percentages of organic (left side) and inorganic (right side) carbon for a spatial subset of the Guadalentin HyMap image. The black areas represent vegetated surfaces that were excluded from the analysis.

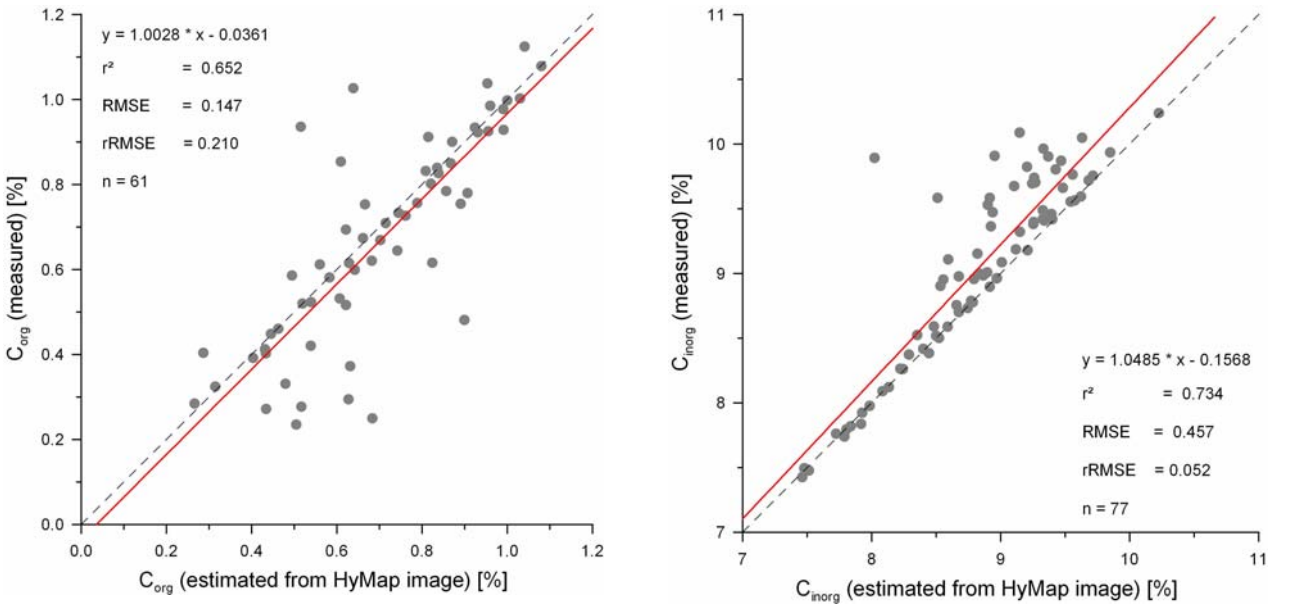

Figure 5: Validation results for the organic (left side) and inorganic (right side) carbon contents estimated from the HyMap image data. The red lines show the linear regression between the modelled and measured values. The dashed lines indicate a linear 1:1-relationship.

It can be concluded that the multivariate regression models applied in this study allow sound estimates of the spatial distribution of soil organic and inorganic carbon concentrations within the test site. The spatially distributed estimates obtained by up-scaling the regression models to the hyperspectral image data follow distinct spatial patterns and thus reflect the local physio-geographic conditions found in the investigated area.

CONCLUSIONS

Organic carbon concentrations were predicted from laboratory reflectance measurements with high accuracy ($r^2_{cv} > 0.79$) based on the C.I.E. chromaticity value y and the C.I.E. tristimulus value Y (luminance). Inorganic carbon was estimated from laboratory reflectance measurements with an accuracy of $r^2_{cv} > 0.71$ considering the normalized absorption area of the carbonate absorption feature at 2.33 µm and the C.I.E. chromaticity value x and y. The up-scaling to HyMap data was successful and reflected the spatial pattern of organic and inorganic carbon concentrations in the investigated area very well. Estimates from HyMap data were verified for organic carbon ($r^2 > 0.65$) and inorganic carbon ($r^2 > 0.73$). Finally it is assumed that the introduced approach is applicable to other semi-arid and arid regions with similar physio-geographic conditions.

ACKNOWLEDGEMENTS

This work was financially supported through the Forschungsfonds of the University of Trier and the LADAMER project (EVK2-CT2002-00179), funded by the European Commission. The computer code for calculating the C.I.E. colour values was kindly provided by R. Escadafal (Cesbio, France). This support is gratefully acknowledged.

REFERENCES

i Reynolds J F & D M Stafford Smith, 2002. Global desertification: do humans cause deserts?, Dahlem Workshop Report 88, Dahlem University Press, Berlin.

ii White D H, 2000. Drought policy, monitoring and management in arid lands. Annals of Arid Zone 39(2): 105-129.

iii Geiger F, 1970. Die Aridität in Südostspanien. (= Stuttgarter Geographische Studien, 77), Stuttgart.

iv Ben-Dor E & A Banin, 1994. Visible and near-infrared (0.4-1.1µm) analysis of arid and semiarid soils. Remote Sensing of Environment 48: 261-274.

v Baumgardner M F, L F Silva, L L Biehl & E R Stoner, 1985. Reflectance properties of soils. Advances in Agronomy, 38: 1-44.

vi Wyszecki G & W S Stiles, 1967. Color Science. Concepts and methods, quantitative data and formulas, New York, London, Sidney.

vii Escadafal R, 1993: Remote sensing of soil color: principles and applications. Remote Sensing Reviews, 7: 261-279.

viii Jarmer T, 2005. Der Einsatz von Reflexionsspektrometrie und Satellitenbilddaten zur Erfassung pedochemischer Eigenschaften in semi-ariden und ariden Gebieten Israels (Trierer Geographische Studien, Heft 29, Trier).

ix Jarmer T, H Lavée, P Sarah & J Hill, 2007. Using reflectance spectroscopy and Landsat data to assess soil inorganic carbon in the Judean Desert (Israel). In: Advances in Remote Sensing and Geoinformation Processing in Land Degradation Assessment, edited by Röder, A & J Hill (ISPRS Book Series, London, Taylor & Francis) (accepted).

x Hunt G R & Salisbury J W, 1971. Visible and near-infrared spectra of minerals and rocks: II. Carbonates. Modern Geology, 2: 23-30.

xi Gaffey S J, 1986. Spectral reflectance of carbonate minerals in the visible and near infrared (0.35-2.55 microns): calcite, aragonite, and dolomite. American Mineralogist, 71: 151-162.

xii Schläpfer D & R Richter, 2002. Geo-atmospheric Processing of Airborne Imaging Spectrometry Data Part 1: Parametric Orthorectification. International Journal of Remote Sensing, 23(13): 2609-2630.

xiii Hill J and B Sturm, 1991. Radiometric correction of multi-temporal Thematic Mapper data for use in agricultural land-cover classification and vegetation monitoring. International Journal of Remote Sensing, 12(7): 1471-1491.

xiv Hill J, W Mehl & V Radeloff, 1995. Improved forest mapping by combining atmospheric and topographic effects, In: Sensors and environmental applications of remote sensing, edited by J Askne (A.A. Balkema: Rotterdam/Brookfield), 143-151.

xv Tanré D, C Deroo, P Duhaut, M Herman, J J Morcrette, J Perbos & P Y Deschamps, 1990. Description of a computer code to simulate the signal in the solar spectrum: the 5S code. International Journal of Remote Sensing, 11, 659-668.

xvi Sobolev V V, 1963. A treatise on radiative transfer, (Van Nostrand: Princeton).

xvii Berk A, G P Anderson, P K Acharya, P K Chetwynd, L S Bernstein, E P Shettle, M W Matthew & S M Adler-Golden, 1999. MODTRAN4 user's manual, Hanscom AFB, MA 01731-3010: Airforce Research Laboratory, Space Vehicles Directorate, Airforce Material Command.

xviii Hill, J, & S Mader, 2007. Estimating continuous vegetation fields in an arid ecosystem using a coupled leaf-canopy reflectance model at different spatial/spectral scales. In: 5th EARSeL SIG IS workshop on "IMAGING SPECTROSCOPY: innovation in environmental research", to appear.

xix Adams J B, M O Smith & A R Gillespie, 1989. Simple methods for complex natural surfaces: a strategy for the hyperspectral era of remote sensing. In: Proc. of the IGARSS Symposium, 10-14 July, IEEE, Vancouver, Canada, 16-21.

xx Roberts D A, M O Smith & J B Adams, 1993. Green vegetation, nonphotosynthetic vegetation, and soils in AVIRIS data. Remote Sensing of Environment 44: 255-269.